

Research article

Role of nanocellulose geometric structures on the properties of green natural rubber composites

Milanta Tom^{1,2}, Sabu Thomas^{1,3,4,5*}, Bastien Seantier², Yves Grohens²,
Mohamed Pulikaparambil Kochaidrew⁶, Ramakrishnan Subramanian⁶,
Tapas Ranjan Mohanty⁶, Henri Vahabi⁷, Hanna Joseph Maria¹, Jibin Keloth Paduvilan⁸,
Martin George Thomas¹

¹School of Energy Materials, Mahatma Gandhi University, 686560 Kottayam, Kerala, India

²University Bretagne Sud, UMR CNRS 6027, IRDL, F-56100 Lorient, France

³School of Nanoscience and Nanotechnology, Mahatma Gandhi University, 686560 Kottayam, Kerala, India

⁴International and Inter-University Centre for Nanoscience and Nanotechnology, Mahatma Gandhi University, 686560 Kottayam, Kerala, India

⁵Department of Chemical Sciences, University of Johannesburg, 17011 Johannesburg, South Africa

⁶Global R&D Centre, Asia, Apollo Tyres Ltd., 602105 Chennai, Tamil Nadu, India

⁷Université de Lorraine, CentraleSupélec, LMOPS, F-57000, Metz, France

⁸School of Chemical Science, Mahatma Gandhi University, 686560 Kottayam, Kerala, India

Received 16 January 2024; accepted in revised form 30 March 2024

Abstract. The augmented demand for sustainable nanocomposites has paved the way to explore naturally derived materials. Nanocellulose, with its bountiful sources and inherent properties, ranks top in the list of biofillers with a perspective of reducing the carbon footprint. A systematic study is required to understand the reinforcing effect of various types of nanocellulose. In the present work, we selected three types of nanocellulose, *i.e.*, cellulose nanocrystal (CNC), cellulose nanofiber (CNF) and microfibrillated cellulose (MFC), to investigate the effect of geometrical structure on the properties of unvulcanized natural rubber (NR). Incorporating these fillers improved the tensile strength and modulus of natural rubber films significantly through reinforcement via filler network structure. The reinforcing effect of CNF was found to be higher compared to CNC and MFC, where an increase of 3.85 MPa in tensile strength from the neat sample was obtained. More uniform dispersion was evident through transmission electron microscopy, atomic force microscopy and Raman imaging for CNF in the rubber matrix. The structural properties were determined using Raman spectra and X-ray diffraction. The rheological studies revealed a good interaction between filler and NR. The work presented comprehensively compares different types of nanocellulose as reinforcing filler in NR matrix, which will help the researchers select an ideal type for their specific application and, thus, the proper usage of renewable resources, leading to sustainability and a circular economy.

Keywords: nanocellulose, natural rubber, reinforcement, nanocellulose geometry, nanofibers, structure- property relationship

1. Introduction

Reinforcing fillers are indispensable in developing rubber composites for high-performance applications. Precipitated silica and carbon black are the primary reinforcing fillers in rubber industries [1]. Although these fillers are efficient in improving the

properties of rubber compounds, intense research is going on to replace the commonly used filler materials, considering their negative impact on the environment and human health [2]. It was estimated that a large amount of energy is consumed (44 GJ/t) during the production of carbon black (CB) with a CO₂

*Corresponding author, e-mail: sabuthomas@mgu.ac.in

© BME-PT

emission of 3.3 tons per ton of CB [3]. Although silica claims to be a greener filler than carbon black, the environmental impact in terms of non-renewable energy use (NREU) was estimated as 66.0–77.3 MJ/kg and global warming potential (GWP100) of 3.48–4.12 kg CO₂ eq/kg [4]. Identifying a sustainable alternative to carbon black and other conventional filler materials like silica is of great interest in mitigating these negative impacts. Thus, raw material selection is an important parameter for developing sustainable materials [5]. The bio-based fillers from the class of polysaccharides and proteins can be exploited positively to meet the composite material requirements and attain sustainability [6]. Materials such as plant fibers (extracted from jute, sisal, flax, *etc.*), biomasses, and agricultural wastes such as rice husk, corn stalk, *etc.*, are being studied for their utilization as additives in rubber composites [7]. The ecological and material concerns have led to the research interest in cellulosic fillers due to their excellent and intriguing properties [8].

Fillers of nanoscale dimensions incorporated in rubbers are more efficient than macrosized fillers in increasing strength, abrasion resistance, UV stability, and other performances [9]. Nanocellulose – cellulose in nanoscale dimensions – has recently evolved as a promising reinforcing filler in the elastomer industry due to its outstanding characteristics such as renewability, biodegradability, availability, lower cost, low density (1.5–1.6 g/cm³) [10], high mechanical strength, high-temperature stability [11], high dielectric constant [12], and low coefficient thermal expansion [13]. The high aspect ratio and large surface area of nanocellulose are ideal for transferring stress from the rubber matrix to the nanocellulose filler [14]. The surface chemistry of nanocellulose can be tailored to establish strong matrix filler interaction [15].

Cellulose nanomaterial can be classified into two categories based on size and morphology [16, 17]. The first one is the cellulose nano-objects, which comprises rod or needle-shaped cellulose nanocrystals (CNC) (with diameter ranging from 5–20 nm and length of 100–500 nm) and cellulose nanofibers (CNF) with dimensions of 4–20 nm × 0.5–2 μm [18, 19]. CNCs are usually extracted by strong acid hydrolysis, which removes the amorphous part of the cellulose, leaving behind highly crystalline structures [20, 21]. CNFs are usually obtained by chemical or enzymatic pretreatments followed by physical

treatments (mechanical nanofibrillation) [22, 23]. CNFs contain amorphous parts and are not as crystalline as CNC. Their dimensions depend on the degree of fibrillation and other pretreatment involved in their extraction [24]. The second category comprises cellulose nanostructured materials, which include microfibrillated cellulose (MFC). The diameter of MFC falls in the range of 10–100 nm and several micrometers in length (0.5–50 μm) [25, 26].

The structure of fillers, specifically geometry, plays a significant role in many aspects, including composite preparation, curing kinetics, crosslinking density and ultimately, the properties of prepared nanocomposites [27]. The properties of nanocellulose, like reinforcing efficiency, vary depending on morphology, geometry and structural differences [28, 29]. Nanofiller geometry can influence interconnectivity within the rubber matrix. The interconnectivity makes the dispersed filler phase a continuous phase within the matrix which was found to increase properties like thermal conductivity [30]. Selection of the ideal type of nanocellulose and tailoring the interface chemistry between nanocellulose and elastomer are obligatory to attain optimum performance as they can influence different properties through filler-polymer and filler-filler interactions [31].

Several studies discuss the efficiency of nanocellulose as a reinforcing filler in natural rubber to improve properties like mechanical, barrier, and thermal stability [26, 32, 33]. Kazemi *et al.* [34] reported that adding nanocellulose to natural rubber resulted in better dynamic mechanical properties than carbon black-reinforced natural rubber composites. Cheng *et al.* [35] observed that the geometry of nanocellulose can affect the properties of composites. However, a detailed investigation of the effect of the geometrical difference of CNC, CNF and MFC on the properties of uncured natural rubber has yet to be reported. The main objective of the work is to look into the influence of geometry and concentration of different types of nanocellulose CNC, CNF and MFC on morphology, rheology and mechanical properties of uncured natural rubber films. A green natural rubber composite system will give a precise account of filler interaction with the rubber matrix. Characterizations of nanocomposite films were carried out by transmission electron microscopy (TEM), atomic force microscopy (AFM) and Raman spectroscopy. Deformation analysis was carried out via amplitude sweep and frequency sweep as a function

of the concentration of nanocellulose. Mechanical properties like tensile strength, modulus and elongation at break [%] were also analyzed and discussed in detail. The results from this study show clear distinctions between short, rigid CNCs, long, relatively tough CNFs and longer MFCs in terms of their reinforcing effects and mechanisms. We illustrate the filler geometry dependence of the properties of nanocomposite films, which is mainly controlled by the dispersion of nanofiller. The work will surely be an excellent tool to guide the selection of an ideal type of nanocellulose with tailored properties to design a material to suit a particular application.

2. Materials and methods

2.1. Materials

Centrifuged natural rubber latex, stabilized with ammonia, with a dry rubber content of 60 wt%, purchased from M/S Kurians Industries, Kottayam, Kerala, India, was used to prepare nanocomposites. Cellulose nanocrystals (CNC) (2 wt%, 1.45 g/cm³) was purchased from ICAR-CIRCOT, Mumbai, India; cellulose nanofibers (CNF) (3 wt%, 1.005 g/cm³) was supplied by Sappi, Maastricht, The Netherlands; microfibrillated cellulose (MFC) (10 wt%, 1.5 g/cm³) was supplied by Borregaard, Sarpsborg, Norway.

2.2. Preparation of nanocomposites

Homogenous and stable dispersion of nanocellulose in an elastomer matrix is the linchpin to efficacious nanocomposite. Nanocellulose was incorporated into the rubber phase utilizing the latex stage processing technique, which is both environment-friendly and cost-effective. The different types of nanocellulose were diluted to 2 wt%. Filler suspensions were homogenized using IKA Ultra-Turrax T25 homogenizer

at 10 000 rpm for ten min. as two cycles. They were slowly added at different concentrations (2.5, 5 and 10 phr) to natural rubber latex under magnetic stirring for two hours. These concentrations of nanocellulose were chosen to gain a basic understanding of how the properties of natural rubber film change with the nanocellulose loading. Mechanical stirring (10 min.) was employed at the final mixing stages to ensure complete dispersion.

The casting procedure was adopted to prepare nanocomposite films of uniform thickness, as shown in Figure 1. In this method, nanocellulose/natural rubber solutions were cast on glass plates and dried in a hot air oven at 40 °C to get dry films of an average thickness of around 2 mm. These films were used to evaluate the influence of nanocellulose geometry on the green strength of natural rubber. (The composite films are noted as NR followed by the type of nanocellulose used, which is then followed by phr used, e.g., NRCNC10).

2.3. Experimental

2.3.1. Characterization techniques

Nanocellulose suspension stability studies – zeta potential and dynamic light scattering (DLS)

The stability of colloids and suspensions can be determined by zeta potential analysis based on the electrostatic repulsive forces on surface charges [36]. Zeta potential of nanocellulose dispersions and their particle sizes were measured using the phase analysis light scattering (PALS) mode on a dynamic light scattering system (Nanoparticle Analyzer, HORIBA SZ-100, Kyoto, Japan) with DPSS 532 nm laser at a temperature of 25 °C. All samples were diluted to attain similar viscosity values (0.89 mPa·s) and the concentration of the solution was 10 mg/ml.

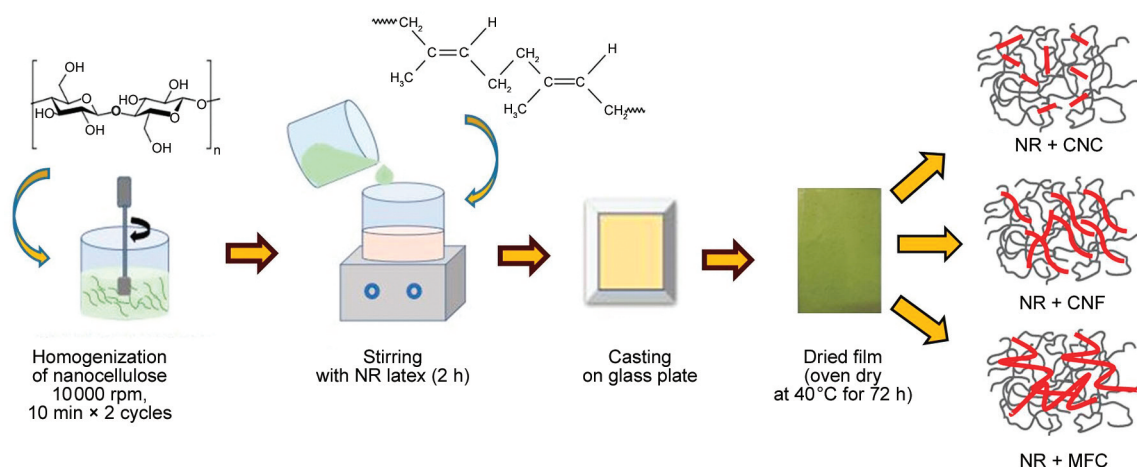


Figure 1. Schematic representation of the preparation of nanocomposite film.

2.3.2. Fourier transform infrared (FTIR) spectroscopy

The FTIR spectra of CNC, CNF and MFC were recorded on FTIR instrument (Perkin-Elmer Spectrum Two FTIR Spectrometer, Massachusetts, United States) in the range of 4000–400 cm^{-1} with a resolution of 4 cm^{-1} to analyze their chemical composition.

2.3.3. Morphological and structural analysis

The dispersion of nanocellulose in the rubber phase was analyzed using the following techniques.

Transmission electron microscopy (TEM)

The analysis was carried out using JEOL JEM 2100 (Tokyo, Japan) (LaB6) high-resolution TEM with an operating voltage of 200 kV. The morphology of nanocellulose was analyzed after proper dilution, followed by sonication to ensure ideal dispersion. A drop of diluted sample was placed on a copper grid and allowed to dry before imaging. The dispersion characteristics of nanocellulose in rubber matrices were analyzed using cryo-microtome sections of nanocomposites. Samples were maintained below their glass transition temperature during cryomicrotomy. The cryo-sections of thickness 100 nm were cut using LEICA EM FC7 (Wetzlar, Germany) equipped with glass knives and were placed directly on copper grid of 300 mesh size for imaging.

Atomic force microscopy (AFM)

The morphology, as well as surface properties of different types of nanocellulose and nanocomposites, were analyzed using the WITec ALPHA 300RA AFM (Ulm, Germany) instrument. Height images were captured to analyze the morphology of CNC, CNF and MFC. To analyze the nanocomposites, measurements were carried out in tapping mode using a silicon nitride tip with a resonance frequency of 75 kHz, force constant of 2.8 N/m and a radius of curvature less than 8 nm. The scanning was done over an area of $5 \times 5 \mu\text{m}$, and phase images were captured.

Raman spectroscopy and imaging

Structural analysis was carried out using confocal Raman microscopy system (WITec ALPHA 300RA, Ulm, Germany) equipped with a 532 nm DPSS laser with a maximum power of 42 mW coupled to a microscope equipped with a $100\times/0.9$ DIC Zeiss (E-Ceipplan-Neofluar) objective, a spectrometer (UHTS 300, focal length 300 mm, with $1800 \text{ g}\cdot\text{mm}^{-1}$ grating),

and a CCD camera. System calibration was performed using a silicon wafer to ensure standard band position and intensity. The Raman spectra were recorded in the spectral range of 20–3500 cm^{-1} .

2.3.4. X-ray diffraction (XRD)

The X-ray diffraction (XRD) patterns were recorded using a Rigaku Miniflex II (Tokyo, Japan) diffractometer with $\text{Cu K}\alpha$ radiation. The scanning range was from 2° to 90° with a step time of 1 s. All measurements were taken using a 30 kV voltage and a 15 mA current. The crystallinity index (*CI*) of nanocellulose was calculated using the Segal empirical equation (Equation (1)) [37]:

$$CI [\%] = \frac{I_{002} - I_{\text{am}}}{I_{002}} \cdot 100 \quad (1)$$

where I_{200} represents the peak diffraction intensity corresponding to crystalline cellulose, and I_{am} is the peak diffraction intensity corresponding to the amorphous sections in nanocellulose [38, 39].

2.3.5. Rheological properties

The rheological properties were analyzed using a stress-controlled rotational rheometer Anton Paar MCR 301 (Graz, Austria) rheometer at 120°C . The nonlinear viscoelastic behavior of nanocomposites has been analyzed via strain sweep and frequency sweep. The strain sweep was carried out by varying shear strain from 0.01 to 100% at a constant frequency of 1 Hz. The angular frequency was varied from 0.001 to 100 rad/s with a shear strain of 0.01% for frequency sweep analysis.

2.3.6. Mechanical properties

The stress-strain properties of different unvulcanized nanocomposite films were studied by uniaxial stretching using a universal testing machine (Tinius Olsen H25KL, Horsham, United States). The testing was performed on dumbbell-shaped specimens with an overall length of 115 mm, gauge length of 25 mm, width of 6 mm and thickness of 2 mm by ASTM D 412 – 06 at a crosshead speed of 500 mm/min.

3. Results and discussion

3.1. Nanocellulose suspension stability studies

The stability of nanocellulose is imperative to prevent aggregation. The repulsive force within nanocellulose should be as high as possible to minimize the interactions leading to aggregation. It has been

Table 1. Zeta potential values of different types of nanocellulose.

Sample name	Zeta potential [mV]	Dispersion medium viscosity [mPa·s]
CNC	-52.2	0.895
CNF	-46.7	0.892
MFC	-50.7	0.894

Table 2. Mean particle size of different types of nanocellulose.

Sample name	Mean particle size [nm]
CNC	5.4
CNF	2.8
MFC	13.3

reported that a zeta potential value higher than 30 mV or lower than -30 mV makes the suspension stable [40–42]. The zeta potential values of CNC, CNF and MFC are given in Table 1. The dispersion medium viscosity of the different nanocellulose samples was measured and found to be similar among them. All three types of nanocellulose showed lower zeta potential values than some of the reported works, where CNC, CNF, and MFC had zeta potentials of -37.8 mV [43], -14.7 mV [44] and -22.3 mV [45], respectively. The results revealed the excellent stability of nanocellulose suspensions used in this research. Table 2 represents the mean particle size of three types of nanocellulose obtained from DLS analysis. It was found that MFC showed the highest particle size followed by CNC and CNF.

3.2. FTIR

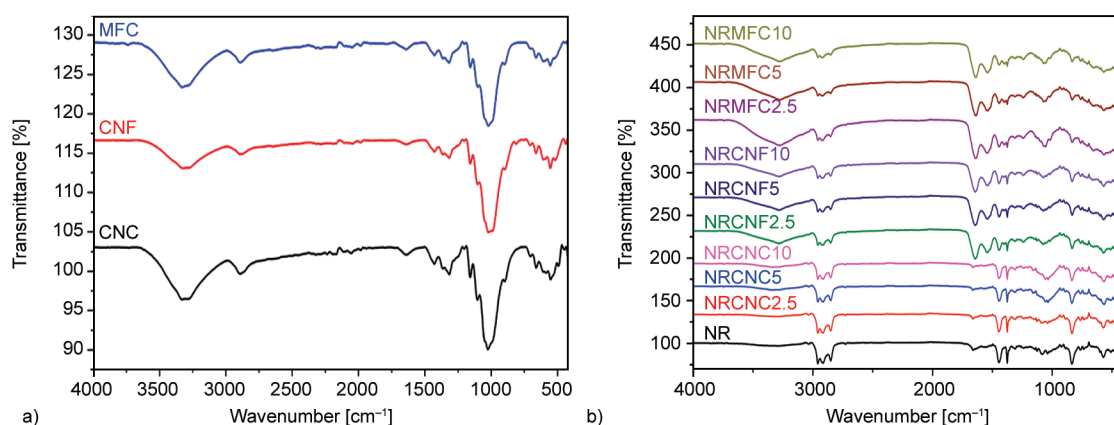
All three types of nanocellulose present almost similar FTIR spectra, suggesting the composition of nanocellulose is the same despite its geometry, as

shown in Figure 2. The broad peak in the range of 3336–3298 cm^{-1} is attributed to -OH stretching and intermolecular hydrogen bonding [46]. The OH stretching of CNC was found to be more pronounced than CNF which may be due to the higher stretching vibration bands of the O-H bonds of primary and secondary hydroxyl groups of CNC [47]. The absorption peak between 2900 and 2800 cm^{-1} is assigned to the stretching of C-H groups of nanocellulose [48]. The peak observed at 1644 cm^{-1} is due to the -OH bending of the adsorbed water [23, 49]. The peak located at 1438 cm^{-1} is due to -CH₂ vibration and C-H stretching [50, 51]. The stretching of C-O is observed at 1032 cm^{-1} [52]. The peak at 896 cm^{-1} is attributed to the C-O-C vibration of glycosidic ether linkage [53, 54]. The FTIR spectra of all the nanocomposites are also shown in Figure 2. The characteristic peak at 836 cm^{-1} is considered as the finger print region of NR. The peak at 2960 cm^{-1} represents the -CH₃ asymmetric stretching, and the peak at 1665 cm^{-1} represents the -C=C- stretching [55]. It was found that the characteristic peaks of nanocellulose are masked by NR in the case of CNC nanocomposites, whereas these peaks are more prominent in the case of nanocomposites of CNF and MFC.

3.3. Morphology and structural analysis:

3.3.1. Transmission electron microscopy (TEM)

It is essential to understand the arrangement of nanofillers within the matrix as it has a strong influence on the properties of nanocomposites [56]. The morphological analysis of nanocellulose revealed that the CNC exhibited needle-like structures, with an average diameter of 20 nm and length of 300 nm. CNF and MFC exhibited highly entangled network-like structures due to their high aspect ratio and semi-crystalline nature [22, 57], with an average diameter

**Figure 2.** FTIR spectra of a) CNC, CNF and MFC b) NR nanocellulose composites.

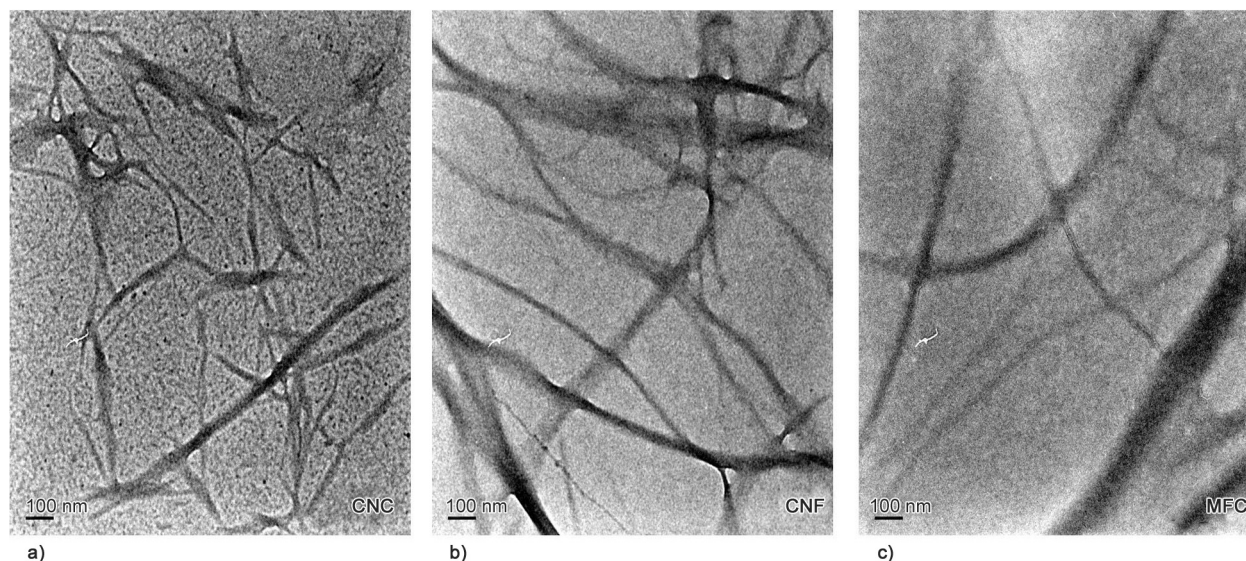


Figure 3. TEM images of different types of nanocellulose, a) CNC, b) CNF, and c) MFC.

of 16 and 32 nm, respectively. The dimensions of nanocellulose were measured using Image J software. **Figure 3** represents the TEM images of different types of nanocellulose. The measurement of the length of individual CNF and MFC with accuracy was difficult due to the entangled fiber structure.

The level of dispersion and presence of agglomeration of nanocellulose in rubber matrices were analyzed using the TEM images of nanocellulose/natural rubber composite film samples. **Figure 4** shows the TEM images of NR (**Figure 4a**) and nanocomposite films. The TEM images of CNC-loaded nanocomposite films are shown in **Figure 4b**. The 10 phr loading of CNC has resulted in agglomeration of fillers, which can be seen as a rough and uneven appearance in NRCNC10.

CNF was found to be more homogeneously distributed within the rubber matrix. Also, the aligned arrangement of CNF in the NR matrix was evident in **Figure 4c**. The alignment of fillers in nanocomposites has a significant effect on mechanical properties [58]. The bridging of CNF within the rubber matrix due to inter-fiber entanglements and hydrogen bonding was also apparent. The continuous path or bridging is assumed due to percolation network formation. This filler bridging or network formation will result in efficient stress transfer from the matrix to the reinforcing filler [59]. **Figure 4d** represents the less uniform distribution of MFC in a rubber matrix with some agglomeration due to their more extended and highly entangled morphology, and this is in agreement with the observations of Bendahou *et al.* [60].

3.3.2. Atomic force microscopy (AFM)

AFM is an important technique for getting an insight into nanofiller dispersion in polymer matrices along with surface topography [61]. The surface features of natural rubber film and its nanocomposites were evaluated using this technique to envisage the effect of different types of nanocellulose. **Figure 5a** represents topographical images of CNC, CNF and MFC. Morphology of all three types of nanocellulose showed a similar trend as in TEM images. AFM images of neat NR and nanocomposites are shown in

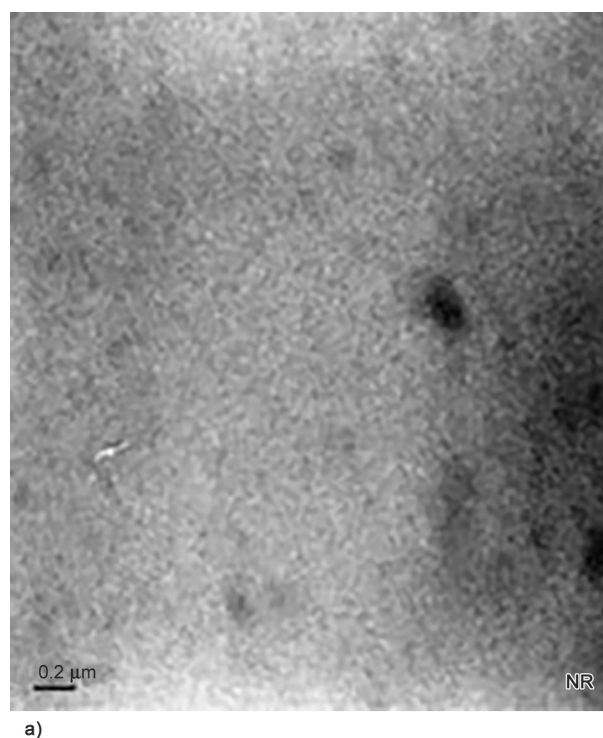


Figure 4. TEM images of a) NR (continued on next page).

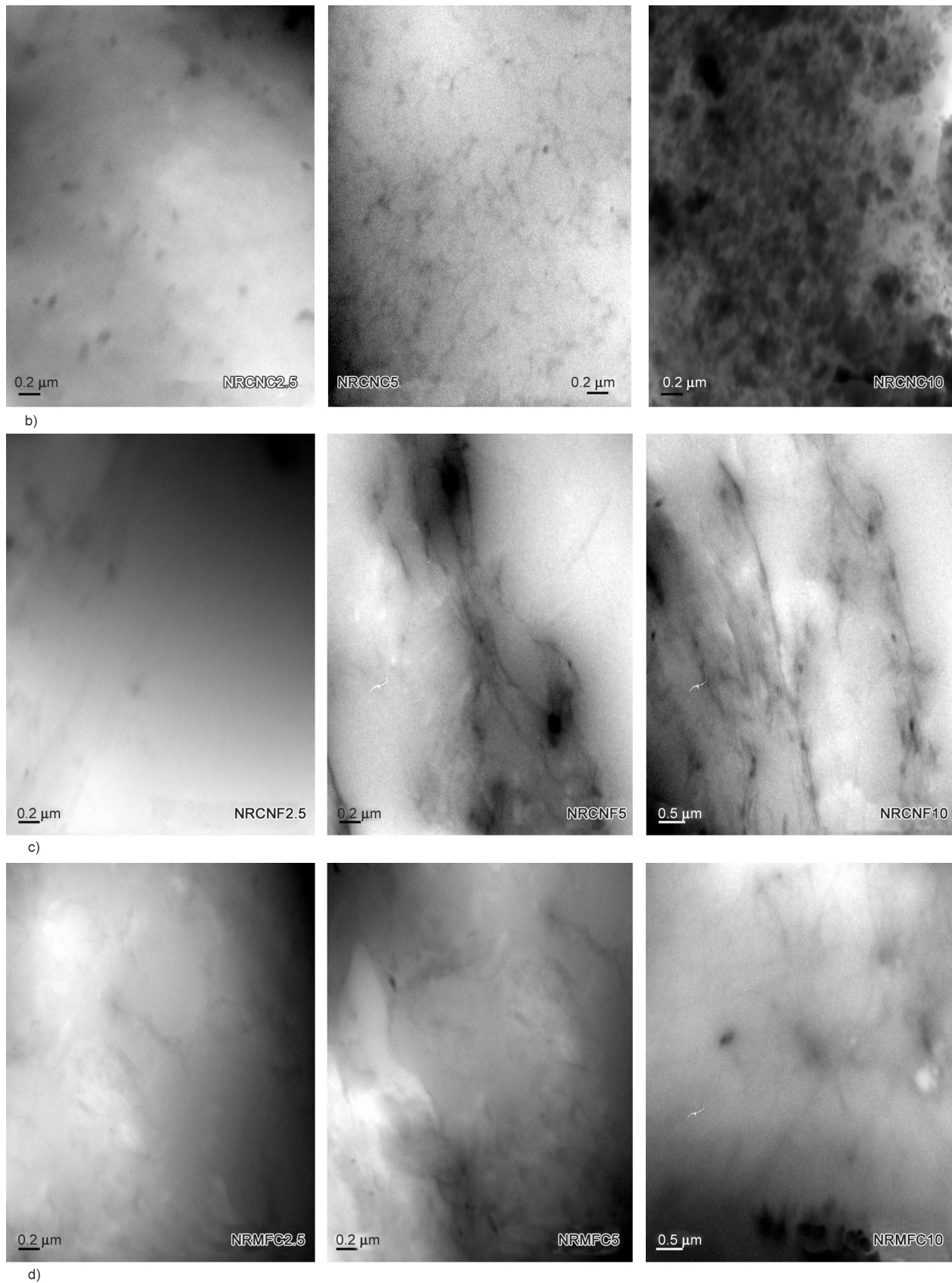


Figure 4. TEM images of b), c), and d) NR nanocomposites.

Figure 5b, respectively). The agglomeration of CNC on the surface of the rubber matrix is quite evident

from the NRCNC10 image. CNF filled nanocomposites represented better filler dispersion within the

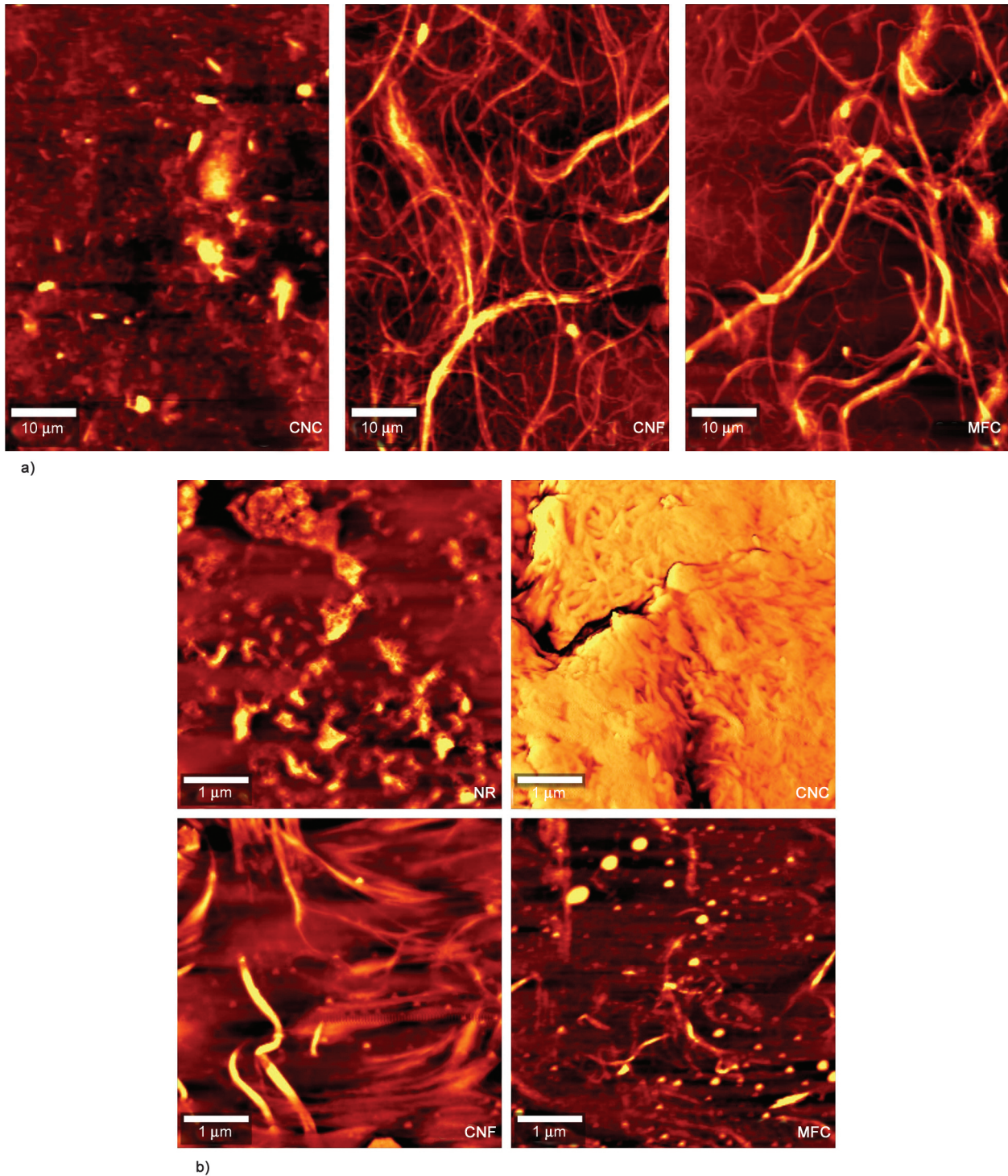


Figure 5. AFM topographical images of a) different types of nanocellulose and b) neat NR and nanocomposites..

matrix, whereas MFC, with its higher aspect ratio, showed a slight tendency to agglomerate as compared to CNF.

The surface features of nanocomposites can be quantified in terms of surface roughness [62]. The surface roughness can be expressed as root mean square roughness (R_q) and the arithmetic roughness average (R_a). R_q represents the square root of the surface height deviation from the mean data, and R_a

represents the mean height calculated over the entire measured area. A higher value of the difference between R_q and R_a confirms the presence of filler particles on the surface of the matrix [63]. The surface roughness values of neat natural rubber film, as well as nanocomposites, are represented in Table 3.

Higher filler agglomeration results in higher values of surface roughness [60]. The CNC-filled nanocomposites showed the highest roughness values, which

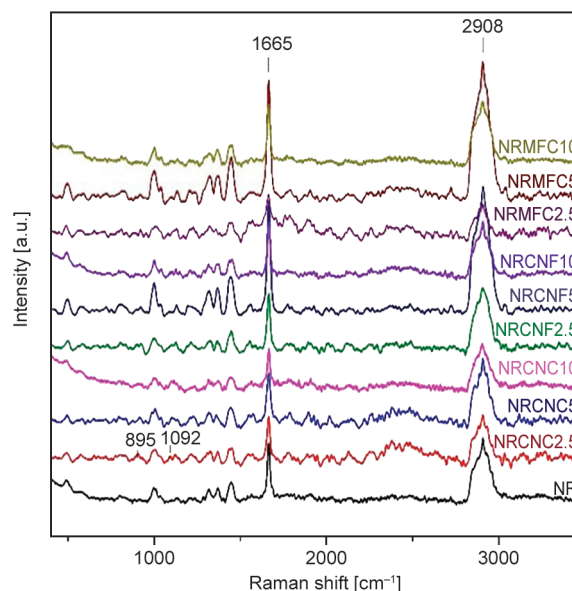
Table 3. Surface roughness values of NR and NR nanocomposites.

Sample name	R_q [nm]	R_a [nm]	$R_q - R_a$ [nm]
NR	27.7	20.7	7.0
NRCNC10	70.4	47.1	23.3
NRCNF10	11.0	8.2	2.9
NRMFC10	12.7	9.7	3.0

may be due to the higher agglomeration tendency of CNC [64], whereas CNF and MFC-filled samples showed lower roughness values, and these observations are in agreement with the TEM and AFM studies. Sharma *et al.* [65] observed a similar decrease in roughness values of NR latex films containing CNF. The better dispersion of CNF in the NR matrix, as well as the partial attachment of CNF molecules with NR chains [66], might have caused this reduction in surface roughness. Roughness values show a close dependence on the particle size as well. The higher the particle size due to agglomeration, the higher will be the surface roughness [67]. CNC particles were agglomerated on the matrix surface, leading to an increase in their average size, thus resulting in higher roughness values compared to other types of nanocellulose. Nanocomposites containing MFC showed roughness values comparable to CNF-filled nanocomposites, which can be attributed to their similar geometrical structure.

3.3.3. Raman spectroscopy and imaging

Raman spectra of natural rubber and natural rubber nanocellulose composites are presented in Figure 6. The Raman spectrum of NR shows two well-defined peaks at 1665 and 2908 cm^{-1} representing C=C stretching and CH_3 symmetric stretching, respectively [68], and no shift in peaks was observed for nanocomposites. The characteristic peak of nanocellulose is usually at 1095–1096 cm^{-1} corresponding to the C–O (carbonyl) stretching mode and glycosidic stretching mode (C–O–C) [69, 70]. The CNC-filled nanocomposite shows this characteristic peak but with a slight shift to 1092 cm^{-1} , which may be due to the interaction with the rubber matrix. Both CNF and MFC-filled composites show lower intensity peaks in the region, which can be attributed to the effective interaction with the matrix [71]. The intensity of this peak is low in all the composites due to the masking effect of the rubber matrix. The peak corresponding to C–O–C and C–O–H at 895 cm^{-1}

**Figure 6.** Raman spectra of NR and NR nanocomposites.

[72, 73] is more prominent in CNC-loaded samples, which has been assumed due to the higher crystallinity of CNC [69] than in CNF and MFC-loaded samples. The differences in the peak intensities may be due to the geometrical structural differences among the three types of nano cellulose [74].

3.4. X-ray diffraction (XRD)

The XRD patterns of CNC, CNF and MFC are shown in Figure 7a. The XRD pattern of all three types of nanocellulose showed characteristic peaks around 2θ at 16.5° and 23°, which corresponds to cellulose type I [41, 75]. These peaks correlate with the lattice planes 101 and 002 [54, 76]. The CNC showed the highest intensity at 23° as compared to CNF and MFC. The removal of amorphous regions during the CNC extraction is probably the reason for the higher crystallinity of CNC than the fibrous nanocellulose [77]. The crystallinity index of CNC, CNF, and MFC are shown in Table 4.

X-ray diffraction analysis of nanocomposites was also performed to investigate the crystallographic nature of the nanocellulose-incorporated NR composites. A shift in the characteristic peaks of nanocellulose is evident from the XRD patterns of nanocomposites given in Figure 7b. This shift can be attributed to the trapped arrangement of nanocellulose molecules within the NR molecular chains [78]. The peak shift towards the lower angle is due to the expansion of the nanocellulose lattice, which may be due to the presence of rubber molecules [79].

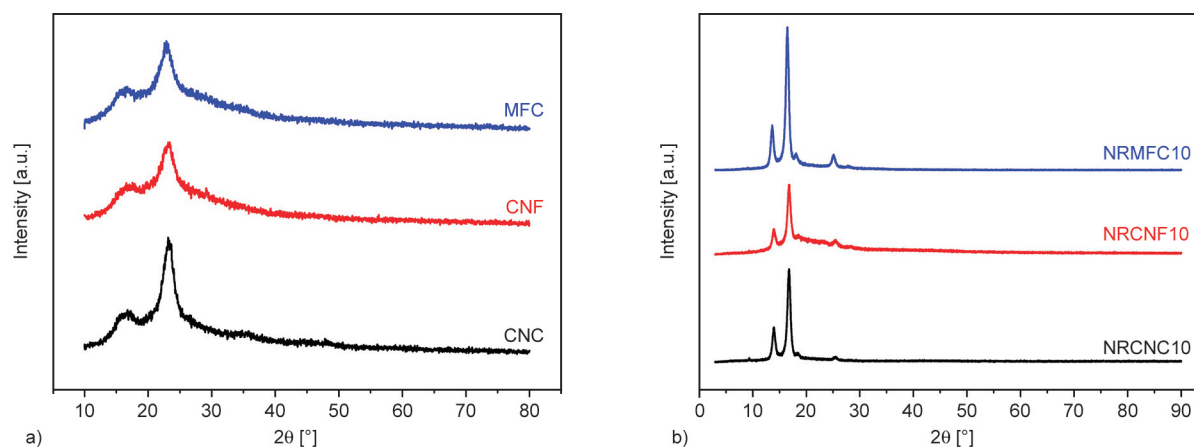


Figure 7. XRD patterns of a) CNC, CNF and MFC, b) NR nanocomposites.

Table 4. The crystallinity index of CNC, CNF, and MFC.

Sample name	Crystallinity index
CNC	57.5
CNF	49.2
MFC	50.7

3.5. Rheological properties

The effects of strain amplitude and frequency on the viscoelastic properties of nanocomposites reinforced with different types of nanocellulose were analyzed. Nanocellulose-reinforced NR composites usually exhibit an increase in storage modulus due to an increase in crosslink density and stiffness [80]. Different nanocellulose-filled rubber composites represented different viscoelastic behaviors owing to the difference in geometry and the level of dispersion. It is evident from Figure 8 that the storage modulus values of nanocellulose-incorporated rubber samples were higher at lower amplitude and decreased with increasing strain amplitude. This is in agreement with the previous experimental results on both unvulcanized and vulcanized rubbers filled with reinforcing fillers [81, 82].

As evident from the morphological analysis, agglomeration of CNC in NR matrix resulted in low storage modulus values of NRCNC nanocomposites (Figure 8a) where the mobility of the rubber chain is not significantly altered resulting in lower modulus values. Fibrous nanocellulose filled NR composites demonstrated higher storage modulus than the neat NR and CNC. Enhancement in storage modulus indicates good dispersion of this nanocellulose in the NR matrix [83]. The storage modulus was highest for NRCNF10 (Figure 8b). CNF functions as distinct reinforcing agents at lower loading, but at higher

loading, they form entangled mesh-like network architectures that offer better reinforcement [84]. The physical adsorption between CNF and NR matrix may be another reason for the increase in the storage modulus [85]. The storage modulus of MFC-loaded samples exhibited an increasing trend only at lower concentrations (2.5 and 5 phr). Agglomeration at higher loading might have resulted in lower storage modulus value at 10 phr MFC loaded nanocomposite films as shown in Figure 8c.

The geometrical structural features and level of dispersion of nanocellulose within the rubber matrix are the key parameters influencing the Payne effect – the breakage and reconstitution of the filler network structure under the influence of strain amplitude [86]. The Payne effect is identified as the drop of storage modulus at high strain amplitude due to the breakdown of the filler-filler network [87]. A nonlinear decrease in storage modulus with increasing strain was observed for unfilled NR sample. This can be attributed to the existence of a secondary network contributed by phospholipid terminal groups and fatty acids [88] in the unfilled rubber [89]. Despite the nanocellulose geometry, it was found that the magnitude of Payne effect ($G'_{0\%} - G'_{100\%}$) increased as the nanocellulose loading increased. $G'_{0\%}$ represents the storage modulus at the plateau of the curve at the lowest strain, and $G'_{100\%}$ is the minimum storage modulus at the highest strain [29]. Thus, the difference between $G'_{0\%}$ and $G'_{100\%}$ can be an indicator about the nanofiller networks that are developed in rubber matrix [90]. The primary cause of the amplified Payne effect is the breakdown of the hydrogen-bonded filler networks at greater loadings of nanocellulose [91]. The loss modulus of the neat NR sample increased at around 10% shear strain due to the increase in

dissipation energy at higher strain [92, 93]. This trend is not exhibited by any of the nanocomposites. As represented in Figure 8, the loss modulus decreases with a further increase in strain amplitude. The higher loadings of nanocellulose restrict polymer segmental motions requiring higher energy for phase transitions and increasing the frictional forces

between filler and matrix, which results in higher energy dissipation in nanocomposites on increasing filler loading as evident from the loss modulus curves [94]. At higher strain amplitudes, all the filler network structures are broken down, and the mechanism of losing energy terminates, lowering the loss modulus values [95].

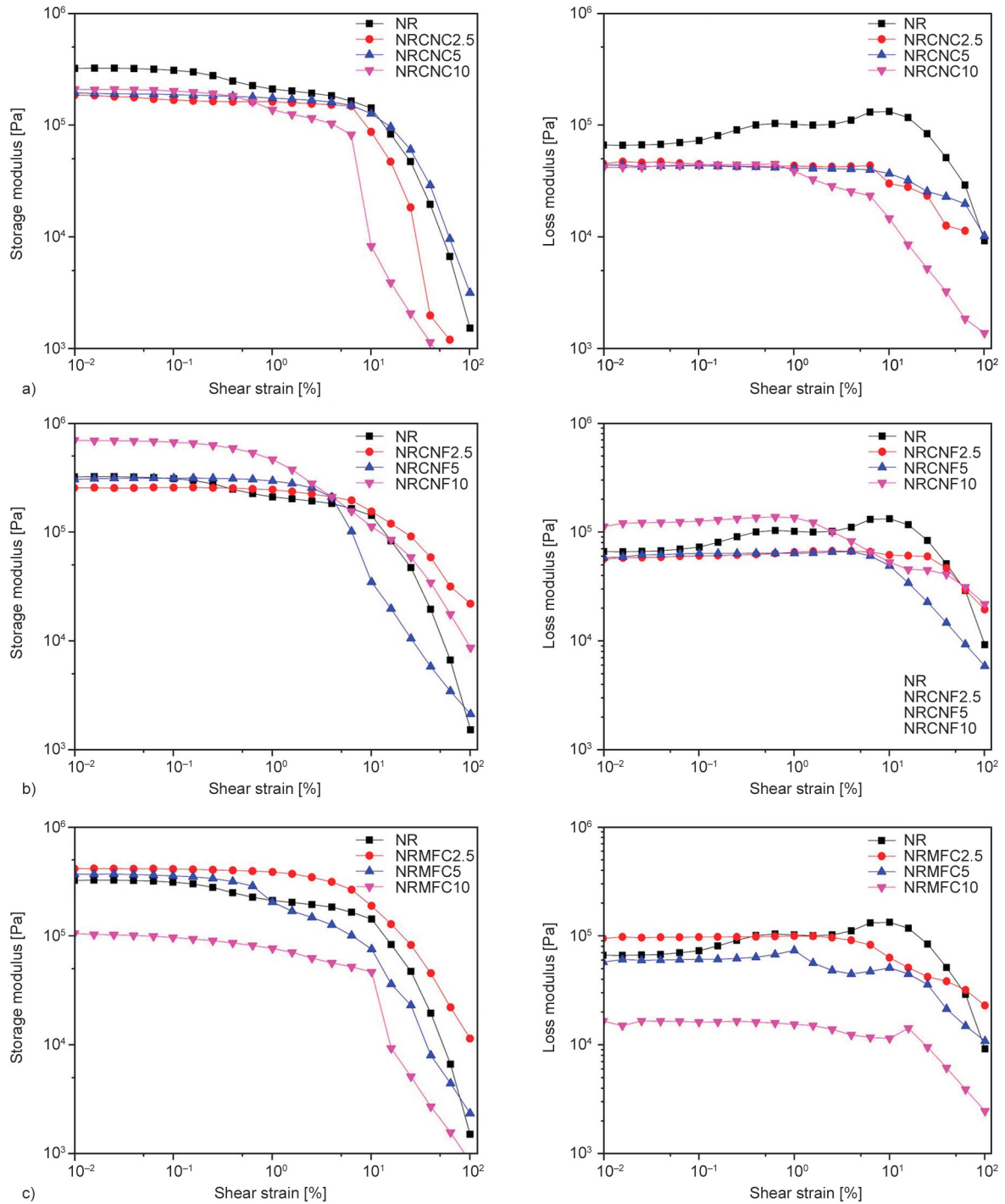


Figure 8. Nonlinear viscoelastic curves of NR and NR nanocellulose composites under amplitude sweep; storage modulus versus shear strain; loss modulus versus shear strain. a) NRCNC nanocomposites, b) NRCNF nanocomposites, c) NRMFC nanocomposites.

3.6. Mechanical properties

Although nanocellulose is an effective reinforcing filler, the reinforcement is ruled by the interfacial interaction and stress transfer between nanocellulose and rubber matrix [96]. The mechanical properties of nanocellulose-reinforced natural rubber films are given in Table 5. It was found that apart from nanofiller loading, the structural geometry of nanocellulose significantly affects mechanical properties. The tensile strength of CNF-based nanocomposites was higher compared to CNC and MFC-based nanocomposites. This enhanced tensile strength can be ascribed to higher entanglement and alignment of CNF molecules, which can lead to the formation of percolation networks [7]. According to Fneich *et al.*, [22] at sufficiently high CNF content, individual nanofibrils contact with each other to form entanglements between flexible amorphous regions or amorphous and crystalline regions of neighboring nanofibril. The combination of higher aspect ratio and hydrogen bonding of fibrillated nanocellulose can enhance the interaction between the filler and matrix through increased hydrogen bonding than CNC [97].

Higher nanocellulose content in the composites restricted the chain mobility, resulting in lower values of elongation at break [98]. The elongation properties of all types of nanocellulose-loaded films were found to be almost similar with a decreasing trend on increasing the loading. The composite films loaded with 10 phr nanocellulose of all geometries have been broken before reaching even 100% elongation. The fibrous fillers exhibited better mechanical properties than crystal geometry, as evidenced by the tensile strength and modulus values. Among the fibrous samples, microfibrillated cellulose-filled samples were found to have higher modulus values than CNF-filled samples, which may be due to their higher

entanglement. Conversely, nanocomposites containing CNC exhibited lower modulus values, which might have resulted from their higher tendency to agglomerate despite their crystallinity. The highly flexible semi-crystalline CNF chains can link or entangle with rubber chains at multiple points, which is impossible for short CNC [99]. Furthermore, long fibers could reach percolation even at low filler contents, and the fiber–fiber interactions due to the percolation network have contributed to further improvement in the mechanical properties of nanocomposites [24].

The magnitude of low strain modulus was observed to be higher in fibrous nanocellulose-loaded rubber composites [100–102], as shown in Figure 9. The observations are in line with previous reports, as fibrous nanocellulose provided greater modulus enhancement at lower strain levels than CNC [61]. The modulus enhancement at lower strain is attributed to effective stress transfer contributed by the aspect ratio of the nanocellulose [9] and filler networking

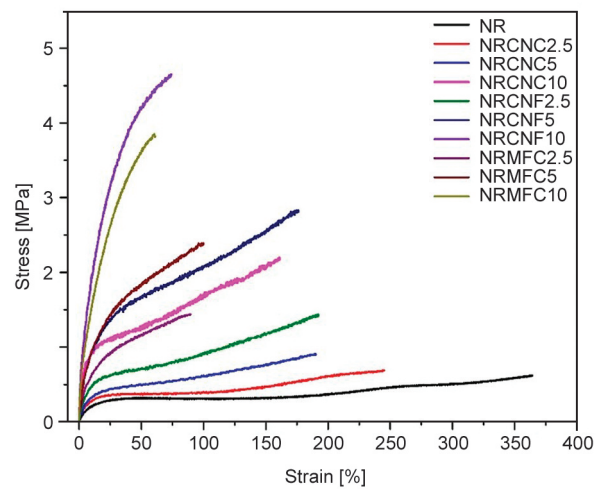


Figure 9. Stress-strain curve of the NR nanocellulose composites.

Table 5. Mechanical properties of NR nanocomposite films.

Sample name	Tensile strength [MPa]	Modulus at 100% elongation [MPa]	Elongation at break [%]
NR	0.60±0.06	0.31±0.00	352±13
NRCNC2.5	0.68±0.07	0.39±0.03	229±11
NRCNC5	0.91±0.08	0.61±0.01	192±15
NRCNC10	1.78±0.08	The sample got broken before 100% elongation	96±7
NRCNF2.5	1.26±0.10	0.99±0.04	190±8
NRCNF5	2.56±0.25	2.06±0.05	167±5
NRCNF10	4.45±0.17	The sample got broken before 100% elongation	74±3
NRMFC2.5	1.29±0.07	1.48±0.03	214±12
NRMFC5	2.29±0.33	2.38±0.08	126±18
NRMFC10	3.85±0.01	The sample got broken before 100% elongation	56±8

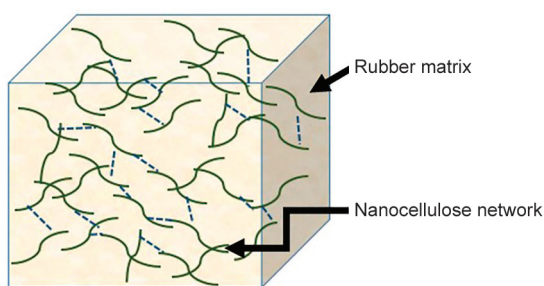


Figure 10. Schematic representation of filler network formation.

[103]. A schematic representation of nanocellulose network formation is given in Figure 10.

It is also reported that other nanofillers with high aspect ratios, like carbon nanotubes, also show similar low-strain modulus enhancement [104]. The agglomeration of CNC in rubber matrix, leading to non-homogenous distribution, has decreased its mechanical properties when compared to fibrous nanocellulose [105].

4. Conclusions

Elastomeric nanocellulose composites have become a new facet in elastomer nanocomposites with extraordinary properties. In this work, sustainable green composite films were successfully prepared and systematically studied to comprehend the effect of different geometry and loading of nanocellulose as reinforcing filler. The geometric contribution of nanocellulose to the properties of natural rubber composites is apparent from morphological, structural, and mechanical behaviors. Although the surface functionalities are the same for CNC, CNF, and MFC, the differences observed in nanocomposites are likely due to the distinct specific surface area, degree of entanglement, aspect ratio, and crystallinity. CNF and MFC showed better dispersion in the rubber matrix from the morphological analysis of TEM and AFM, whereas CNC showed higher crystallinity than both CNF and MFC. This may be due to the removal of amorphous parts during the extraction of CNC. Higher agglomeration of CNC in rubber matrix has resulted in higher surface roughness values than the fibrous nanocellulose. With the increase in the loading of nanocellulose, all the selected geometries represented an increasing trend in mechanical properties. Cellulose nanofibers outperformed all other types of nanocellulose studied in terms of tensile strength – where an increase of 3.85 MPa from the neat sample was obtained and in rheological behavior due to

the formation of an effective filler network. The improvement in properties for fibrous nanocellulose is mainly due to their higher aspect ratio, which helps form interlocking and entanglements of the filler system with rubber chains, higher interfacial area, and increased interaction between matrix and filler. Thus, the principal reinforcement mechanism of nanocellulose in green or unvulcanized rubber matrix is the physical entanglement augmented by the network structure to anchor to rubber chains. The strong dependence of the properties of nanocellulose on the geometry, crystallinity and filler dispersion has to be considered for its use as reinforcing filler in polymeric matrices. The studies based on this virtually inexhaustible reinforcing filler will reshape the elastomer processing strategies towards a more environmentally friendly aspect and a radical influence on the scientific community and industry.

Acknowledgements

The authors gratefully acknowledge the financial support from Global R&D Centre, Asia, Apollo Tyres Ltd. The authors thank Indian Science Technology and Engineering Facilities Map (I-STEM), a Program supported by the Office of the Principal Scientific Adviser to the Govt. of India, for enabling access to the Confocal Raman Microscope with AFM, making WITec, Model: Alpha 300RA, at Sophisticated Analytical Instrument Facilities (SAIF) MGU Kottayam to carry out this work.

References

- [1] Song K.: Interphase characterization in rubber nanocomposites. in 'Progress in rubber nanocomposites' (eds.: Thomas S., Maria H. J.) Elsevier, Amsterdam, 115–152 (2017).
<https://doi.org/10.1016/B978-0-08-100409-8.00004-8>
- [2] Sinclair A., Zhou X., Tangpong S., Bajwa D. S., Quadir M., Jiang L.: High-performance styrene-butadiene rubber nanocomposites reinforced by surface-modified cellulose nanofibers. *ACS Omega*, **4**, 13189–13199 (2019).
<https://doi.org/10.1021/acsomega.9b01313>
- [3] Chikri Y. A., Wetyels W.: Decarbonization options for the Dutch carbon black industry. PBL Netherlands Environmental Assessment Agency, Hague (2020).
- [4] Roes A. L., Tabak L. B., Shen L., Nieuwlaar E., Patel M. K.: Influence of using nanoobjects as filler on functionality-based energy use of nanocomposites. *Journal of Nanoparticle Research*, **12**, 2011–2028 (2010).
<https://doi.org/10.1007/s11051-009-9819-3>
- [5] Ljungberg L. Y.: Materials selection and design for development of sustainable products. *Materials Design*, **28**, 466–479 (2007).
<https://doi.org/10.1016/j.matdes.2005.09.006>

- [6] Palaganas N. B., Palaganas J. O., Doroteo S. H. Z., Millare J. C.: Covalently functionalized cellulose nanocrystal-reinforced photocurable thermosetting elastomer for 3D printing application. *Additive Manufacturing*, **61**, 103295 (2023).
<https://doi.org/10.1016/j.addma.2022.103295>
- [7] Chang B. P., Gupta A., Muthuraj R., Mekonnen T. H.: Bioresourced fillers for rubber composite sustainability: Current development and future opportunities. *Green Chemistry*, **23**, 5337–5378 (2021).
<https://doi.org/10.1039/d1gc01115d>
- [8] Ganapathy V., Muthukumaran G., Sudhagar P. E., Rashedi A., Norrahim M. N. F., Ilyas R. A., Goh K. L., Jawaid M., Naveen J.: Mechanical properties of cellulose-based multiscale composites: A review. *Polymer Composites*, **44**, 734 (2023).
<https://doi.org/10.1002/pc.27175>
- [9] Crosby A. J., Lee J.-Y.: Polymer nanocomposites: The ‘nano’ effect on mechanical properties. *Polymer Reviews*, **47**, 217–229 (2007).
<https://doi.org/10.1080/15583720701271278>
- [10] Dufresne A.: Nanocellulose: A new ageless bionanomaterial. *Materials Today*, **16**, 220–227 (2013).
<https://doi.org/10.1016/j.mattod.2013.06.004>
- [11] Teixeira L. T., Braz W. F., de Siqueira R. N. C., Pandoli O. G., Geraldes M. C.: Sulfated and carboxylated nanocellulose for Co⁺² adsorption. *Journal of Materials Research and Technology*, **15**, 434–447 (2021).
<https://doi.org/10.1016/j.jmrt.2021.07.123>
- [12] Wang J., Liu X., Jin T., He H., Liu L.: Preparation of nanocellulose and its potential in reinforced composites: A review. *Journal of Biomaterials Science, Polymer Edition*, **30**, 919–946 (2019).
<https://doi.org/10.1080/09205063.2019.1612726>
- [13] Guan Q-F., Yang H-B., Han Z-M., Zhou L-C., Zhu Y-B., Ling Z-C., Jiang H-B., Wang P-F., Ma T., Wu H-A., Yu S-H.: Lightweight, tough, and sustainable cellulose nanofiber-derived bulk structural materials with low thermal expansion coefficient. *Science Advances*, **6**, eaaz1114 (2020).
<https://doi.org/10.1126/sciadv.aaz1114>
- [14] Tanpichai S., Thongdeelerd C., Chantaramanee T., Boonmahitthisud A.: Property enhancement of epoxidized natural rubber nanocomposites with water hyacinth-extracted cellulose nanofibers. *International Journal of Biological Macromolecules*, **234**, 123741 (2023).
<https://doi.org/10.1016/j.ijbiomac.2023.123741>
- [15] Kazemi H., Mighri F., Park K. W., Frikha S., Rodrigue D.: Effect of cellulose fiber surface treatment to replace carbon black in natural rubber hybrid composites. *Rubber Chemistry and Technology*, **95**, 128–146 (2021).
<https://doi.org/10.5254/rct.21.78988>
- [16] Poulouse A., Parameswaranpillai J., George J. J., Gopi J. A., Krishnasamy S., Dominic C. D. M., Hameed N., Salim N. V., Radoor S., Sienkiewicz N.: Nanocellulose: A fundamental material for science and technology applications. *Molecules*, **27**, 8032 (2022).
<https://doi.org/10.3390/molecules27228032>
- [17] EN ISO 20477: Nanotechnologies – Vocabulary for cellulose nanomaterial (2023).
- [18] Abitbol T., Rivkin A., Cao Y., Nevo Y., Abraham E., Ben-Shalom T., Lapidot S., Shoseyov O.: Nanocellulose, a tiny fiber with huge applications. *Current Opinion in Biotechnology*, **39**, 76–88 (2016).
<https://doi.org/10.1016/j.copbio.2016.01.002>
- [19] Morais J. P. S., de Freitas Rosa M., de Sá Moreira de Souza Filho M., Nascimento L. D., do Nascimento D. M., Cassales A. R.: Extraction and characterization of nanocellulose structures from raw cotton linter. *Carbohydrate Polymers*, **91**, 229–235 (2013).
<https://doi.org/10.1016/j.carbpol.2012.08.010>
- [20] Habibi Y., Lucia L. A., Rojas O. J.: Cellulose nanocrystals: Chemistry, self-assembly, and applications. *Chemical Reviews*, **110**, 3479–3500 (2010).
<https://doi.org/10.1021/cr900339w>
- [21] Rana A. K., Guleria S., Gupta V. K., Thakur V. K.: Cellulosic pine needles-based biorefinery for a circular bioeconomy. *Bioresource Technology*, **367**, 128255 (2023).
<https://doi.org/10.1016/j.biortech.2022.128255>
- [22] Fneich F., Ville J., Seantier B., Aubry T.: Structure and rheology of aqueous suspensions and hydrogels of cellulose nanofibrils: Effect of volume fraction and ionic strength. *Carbohydrate Polymers*, **211**, 315–321 (2019).
<https://doi.org/10.1016/j.carbpol.2019.01.099>
- [23] Jonoobi M., Oladi R., Davoudpour Y., Oksman K., Dufresne A., Hamzeh Y., Davoodi R.: Different preparation methods and properties of nanostructured cellulose from various natural resources and residues: A review. *Cellulose*, **22**, 935–969 (2015).
<https://doi.org/10.1007/s10570-015-0551-0>
- [24] Xu X., Liu F., Jiang L., Zhu J. Y., Haagensohn D., Wiesenborn D. P.: Cellulose nanocrystals vs. cellulose nanofibrils: A comparative study on their microstructures and effects as polymer reinforcing agents. *ACS Applied Materials and Interfaces*, **5**, 2999–3009 (2013).
<https://doi.org/10.1021/am302624t>
- [25] Bharimalla A. K., Deshmukh S. P., Patil P. G., Vigneshwaran N.: Energy efficient manufacturing of nanocellulose by chemo- and bio-mechanical processes: A review. *World Journal of Nano Science and Engineering*, **5**, 204–212 (2015).
<https://doi.org/10.4236/wjnse.2015.54021>
- [26] Kargazadeh H., Huang J., Lin N., Ahmad I., Mariano M., Dufresne A., Thomas S., Gałęski A.: Recent developments in nanocellulose-based biodegradable polymers, thermoplastic polymers, and porous nanocomposites. *Progress in Polymer Science*, **87**, 197–227 (2018).
<https://doi.org/10.1016/j.progpolymsci.2018.07.008>

- [27] Andrew J. J., Dhakal H. N.: Sustainable biobased composites for advanced applications: Recent trends and future opportunities – A critical review. *Composites Part C: Open Access*, **7**, 100220 (2022).
<https://doi.org/10.1016/j.jcomc.2021.100220>
- [28] Balakrishnan P., Gopi S., Geethamma V. G., Kalarikkal N., Thomas S.: Cellulose nanofiber vs. nanocrystals from pineapple leaf fiber: A comparative studies on reinforcing efficiency on starch nanocomposites. *Macromolecular Symposia*, **380**, 1800102 (2018).
<https://doi.org/10.1002/masy.201800102>
- [29] Camargos C. H. M., Rezende C. A.: Structure–property relationships of cellulose nanocrystals and nanofibrils: Implications for the design and performance of nanocomposites and all-nanocellulose systems. *ACS Applied Nano Materials*, **4**, 10505–10518 (2021).
<https://doi.org/10.1021/acsanm.1c02008>
- [30] Smith D. K., Pantoya M. L.: Effect of nanofiller shape on effective thermal conductivity of fluoropolymer composites. *Composites Science and Technology*, **118**, 251–256 (2015).
<https://doi.org/10.1016/j.compscitech.2015.09.010>
- [31] Presto D., Meyerhofer J., Kippenbrock G., Narayanan S., Ilavsky J., Moctezuma S., Sutton M., Foster M. D.: Influence of silane coupling agents on filler network structure and stress-induced particle rearrangement in elastomer nanocomposites. *ACS Applied Materials and Interfaces*, **12**, 47891–47901 (2020).
<https://doi.org/10.1021/acsami.0c12106>
- [32] Tom M., Thomas S., Seantier B., Grohens Y., Mohamed P. K., Haponiuk J. T., Kim J.: Approaching sustainability: Nanocellulose reinforced elastomers – A review. *Rubber Chemistry and Technology*, **95**, 515–549 (2022).
<https://doi.org/10.5254/rtc.22.77013>
- [33] Cao L., Huang J., Fan J., Gong Z., Xu C., Chen Y.: Nanocellulose-A sustainable and efficient nanofiller for rubber nanocomposites: From reinforcement to smart soft materials. *Polymer Reviews*, **62**, 549–584 (2022).
<https://doi.org/10.1080/15583724.2021.2001004>
- [34] Kazemi H., Mighri F., Park K. W., Frikha S., Rodrigue D.: Natural rubber biocomposites reinforced with cellulose nanocrystals/lignin hybrid fillers. *Polymer Composites*, **43**, 5442–5453 (2022).
<https://doi.org/10.1002/pc.26846>
- [35] Cheng G., Zhou M., Wei Y.-J., Cheng F., Zhu P.-X.: Comparison of mechanical reinforcement effects of cellulose nanocrystal, cellulose nanofiber, and microfibrillated cellulose in starch composites. *Polymer Composites*, **40**, E365–E372 (2019).
<https://doi.org/10.1002/pc.24685>
- [36] Beyene D., Chae M., Dai J., Danumah C., Tosto F., Demesa A. G., Bressler D. C.: Characterization of cellulase-treated fibers and resulting cellulose nanocrystals generated through acid hydrolysis. *Materials*, **11**, 1272 (2018).
<https://doi.org/10.3390/ma11081272>
- [37] Segal L., Creely J. J., Martin A. E., Conrad C. M.: An empirical method for estimating the degree of crystallinity of native cellulose using the X-ray diffractometer. *Textile Research Journal*, **29**, 786–794 (1959).
<https://doi.org/10.1177/004051755902901003>
- [38] Liu P., Sehaqui H., Tingaut P., Wichser A., Oksman K., Mathew A. P.: Cellulose and chitin nanomaterials for capturing silver ions (Ag⁺) from water via surface adsorption. *Cellulose*, **21**, 449–461 (2014).
<https://doi.org/10.1007/s10570-013-0139-5>
- [39] Meng F., Wang G., Du X., Wang Z., Xu S., Zhang Y.: Extraction and characterization of cellulose nanofibers and nanocrystals from liquefied banana pseudo-stem residue. *Composites Part B: Engineering*, **160**, 341–347 (2019).
<https://doi.org/10.1016/j.compositesb.2018.08.048>
- [40] Khatun M. A., Sultana S., Islam Z., Kabir M. S., Hossain M. S., Nur H. P., Chowdhury A. M. S.: Extraction of crystalline nanocellulose (CNC) from date palm mat fibers and its application in the production of nanocomposites with polyvinyl alcohol and polyvinylpyrrolidone blended films. *Results in Engineering*, **17**, 101031 (2023).
<https://doi.org/10.1016/j.rineng.2023.101031>
- [41] Leite A. L. M. P., Zanon C. D., Menegalli F. C.: Isolation and characterization of cellulose nanofibers from cassava root bagasse and peelings. *Carbohydrate Polymers*, **157**, 962–970 (2017).
<https://doi.org/10.1016/j.carbpol.2016.10.048>
- [42] Lin T., Wang Q., Zheng X., Chang Y., Cao H., Zheng Y.: Investigation of the structural, thermal, and physicochemical properties of nanocelluloses extracted from bamboo shoot processing byproducts. *Frontiers in Chemistry*, **10**, 922437 (2022).
<https://doi.org/10.3389/fchem.2022.922437>
- [43] Naduparambath S., Jinita T. V., Shaniba V., Sreejith M. P., Balan A. K., Purushothaman E.: Isolation and characterisation of cellulose nanocrystals from sago seed shells. *Carbohydrate Polymers*, **180**, 13–20 (2018).
<https://doi.org/10.1016/j.carbpol.2017.09.088>
- [44] Huang P., Zhao Y., Kuga S., Wu M., Huang Y.: A versatile method for producing functionalized cellulose nanofibers and their application. *Nanoscale*, **8**, 3753–3759 (2016).
<https://doi.org/10.1039/c5nr08179c>
- [45] Raj P., Blanco A., de la Fuente E., Batchelor W., Negro C., Garnier G.: Microfibrillated cellulose as a model for soft colloid flocculation with polyelectrolytes. *Colloids and Surfaces A: Physicochemical and Engineering Aspects*, **516**, 325–335 (2017).
<https://doi.org/10.1016/j.colsurfa.2016.12.055>
- [46] Jonoobi M., Harun J., Mathew A. P., Hussein M. Z. B., Oksman K.: Preparation of cellulose nanofibers with hydrophobic surface characteristics. *Cellulose*, **17**, 299–307 (2010).
<https://doi.org/10.1007/s10570-009-9387-9>

- [47] Nassiri S., Chen Z., Jian G., Zhong T., Haider M. M., Li H., Fernandez C., Sinclair M., Varga T., Fifield L. S., Wolcott M.: Comparison of unique effects of two contrasting types of cellulose nanomaterials on setting time, rheology, and compressive strength of cement paste. *Cement and Concrete Composites*, **123**, 104201 (2021).
<https://doi.org/10.1016/j.cemconcomp.2021.104201>
- [48] Khalil H. P. S. A., Davoudpour Y., Islam N., Mustapha A., Sudesh K., Dungani R., Jawaid M.: Production and modification of nanofibrillated cellulose using various mechanical processes: A review. *Carbohydrate Polymers*, **99**, 649–665 (2014).
<https://doi.org/10.1016/j.carbpol.2013.08.069>
- [49] Li M., He B., Chen Y., Zhao L.: Physicochemical properties of nanocellulose isolated from cotton stalk waste. *ACS Omega*, **6**, 25162–25169 (2021).
<https://doi.org/10.1021/acsomega.1c02568>
- [50] Gond R. K., Gupta M. K., Jawaid M.: Extraction of nanocellulose from sugarcane bagasse and its characterization for potential applications. *Polymer Composites*, **42**, 5400–5412 (2021).
<https://doi.org/10.1002/pc.26232>
- [51] Theivasanthi T., Christma F. L. A., Toyin A. J., Gopinath S. C. B., Ravichandran R.: Synthesis and characterization of cotton fiber-based nanocellulose. *International Journal of Biological Macromolecules*, **109**, 832–836 (2018).
<https://doi.org/10.1016/j.ijbiomac.2017.11.054>
- [52] Deepa B., Abraham E., Cordeiro N., Mozetic M., Mathew A. P., Oksman K., Faria M., Thomas S., Pothan L. A.: Utilization of various lignocellulosic biomass for the production of nanocellulose: A comparative study. *Cellulose*, **22**, 1075–1090 (2015).
<https://doi.org/10.1007/s10570-015-0554-x>
- [53] Dai H., Ou S., Huang Y., Huang H.: Utilization of pineapple peel for production of nanocellulose and film application. *Cellulose*, **25**, 1743–1756 (2018).
<https://doi.org/10.1007/s10570-018-1671-0>
- [54] Mandal A., Chakrabarty D.: Isolation of nanocellulose from waste sugarcane bagasse (SCB) and its characterization. *Carbohydrate Polymers*, **86**, 1291–1299 (2011).
<https://doi.org/10.1016/j.carbpol.2011.06.030>
- [55] Ibrahim S., Daik R., Abdullah I.: Functionalization of liquid natural rubber *via* oxidative degradation of natural rubber. *Polymers*, **6**, 2928–2941 (2014).
<https://doi.org/10.3390/polym6122928>
- [56] Zhang X., Xiong R., Kang S., Yang Y., Tsukruk V. V.: Alternating stacking of nanocrystals and nanofibers into ultrastrong chiral biocomposite laminates. *ACS Nano*, **14**, 14675–14685 (2021).
<https://doi.org/10.1021/acsnano.0c06192>
- [57] Signori-Iamin G., Santos A. F., Corazza M. L., Aguado R., Tarrés Q., Delgado-Aguilar M.: Prediction of cellulose micro/nanofiber aspect ratio and yield of nanofibrillation using machine learning techniques. *Cellulose*, **29**, 9143–9162 (2022).
<https://doi.org/10.1007/s10570-022-04847-5>
- [58] Zhang H., Zhu L., Zhang F., Yang M.: Effect of fiber content and alignment on the mechanical properties of 3D printing cementitious composites. *Materials*, **14**, 2223 (2021).
<https://doi.org/10.3390/ma14092223>
- [59] Isogai A., Zhou Y.: Diverse nanocelluloses prepared from TEMPO-oxidized wood cellulose fibers: Nanonetworks, nanofibers, and nanocrystals. *Current Opinion in Solid State and Materials Science*, **23**, 101–106 (2019).
<https://doi.org/10.1016/j.cossms.2019.01.001>
- [60] Bendahou A., Kaddami H., Dufresne A.: Investigation on the effect of cellulosic nanoparticles' morphology on the properties of natural rubber based nanocomposites. *European Polymer Journal*, **46**, 609–620 (2010).
<https://doi.org/10.1016/j.eurpolymj.2009.12.025>
- [61] Maiti M., Bhowmick A. K.: New insights into rubber-clay nanocomposites by AFM imaging. *Polymer*, **47**, 6156–6166 (2006).
<https://doi.org/10.1016/j.polymer.2006.06.032>
- [62] Kumar B. R., Rao T. S.: AFM studies on surface morphology, topography and texture of nanostructured zinc aluminum oxide thin films. *Digest Journal of Nanomaterials and Biostructures*, **7**, 1881–1889 (2012).
- [63] George S. C., Rajan R., Aprem A. S., Thomas S., Kim S. S.: The fabrication and properties of natural rubber-clay nanocomposites. *Polymer Testing*, **51**, 165–173 (2016).
<https://doi.org/10.1016/j.polymertesting.2016.03.010>
- [64] Oláh A., Hillborg H., Vancso G. J.: Hydrophobic recovery of UV/ozone treated poly(dimethylsiloxane): Adhesion studies by contact mechanics and mechanism of surface modification. *Applied Surface Science*, **239**, 410–423 (2005).
<https://doi.org/10.1016/j.apsusc.2004.06.005>
- [65] Sharma S. K., Sharma P. R., Lin S., Chen H., Johnson K., Wang R., Borges W., Zhan C., Hsiao B. S.: Reinforcement of natural rubber latex using jute carboxycellulose nanofibers extracted using nitro-oxidation method. *Nanomaterials*, **10**, 706 (2020).
<https://doi.org/10.3390/nano10040706>
- [66] Janík R., Labaj I., Skalková P., Kohutiar M., Mičicová Z., Eckert M.: Influence of filler on structural and surface properties of elastomeric composites. *NanoWorld Journal*, **8**, 96–102 (2022).
<https://doi.org/10.17756/nwj.2022-106>
- [67] Marghalani H. Y.: Effect of filler particles on surface roughness of experimental composite series. *Journal of Applied Oral Science*, **18**, 59–67 (2010).
<https://doi.org/10.1590/S1678-77572010000100011>

- [68] Jansomboon W., Prapainainar P., Loykulnant S., Kongkachuichay P., Dittanet P., Kumnorkaew P., Li Z., Kinloch I., Young R. J.: Raman spectroscopic study of reinforcement mechanisms of electron beam radiation crosslinking of natural rubber composites filled with graphene and silica/graphene mixture prepared by latex mixing. *Composites Part C: Open Access*, **3**, 100049 (2020).
<https://doi.org/10.1016/j.jcomc.2020.100049>
- [69] Agarwal U. P.: Raman spectroscopy of CNC- and CNF-based nanocomposites. in 'Handbook of nanocellulose and cellulose nanocomposites' (eds.: Kargarzadeh H., Ahmad I., Thomas S., Dufresne A.) Wiley, Weinheim, 609–625 (2017).
<https://doi.org/10.1002/9783527689972.ch18>
- [70] Eichhorn S. J., Dufresne A., Aranguren M., Marcovich N. E., Capadona J. R., Rowan S. J., Weder C., Thielemans W., Roman M., Renneckar S., Gindl W., Veigel S., Keckes J., Yano H., Abe K., Nogi M., Nakagaito A. N., Mangalam A., Simonsen J., Benight A. S., Bismarck A., Berglund L. A., Peijs T.: Review: Current international research into cellulose nanofibres and nanocomposites. *Journal of Materials Science*, **45**, 1–33 (2010).
<https://doi.org/10.1007/s10853-009-3874-0>
- [71] Bokobza L., Bruneel J-L., Couzi M.: Raman spectra of carbon-based materials (from graphite to carbon black) and of some silicone composites. *Carbon*, **1**, 77–94 (2015).
<https://doi.org/10.3390/c1010077>
- [72] Bokobza L., Couzi M., Bruneel J-L.: Raman spectroscopy of polymer-carbon nanomaterial composites. *Rubber Chemistry and Technology*, **90**, 37–59 (2017).
<https://doi.org/10.5254/rtc.16.83759>
- [73] Hettrich K., Pinnow M., Volkert B., Passauer L., Fischer S.: Novel aspects of nanocellulose. *Cellulose*, **21**, 2479–2488 (2014).
<https://doi.org/10.1007/s10570-014-0265-8>
- [74] Berglund L., Noël M., Aitomäki Y., Öman T., Oksman K.: Production potential of cellulose nanofibers from industrial residues: Efficiency and nanofiber characteristics. *Industrial Crops and Products*, **92**, 84–92 (2016).
<https://doi.org/10.1016/j.indcrop.2016.08.003>
- [75] Daicho K., Kobayashi K., Fujisawa S., Saito T.: Crystallinity-independent yet modification-dependent true density of nanocellulose. *Biomacromolecules*, **21**, 939–945 (2020).
<https://doi.org/10.1021/acs.biomac.9b01584>
- [76] Ho T. T. T., Zimmermann T., Hauert R., Caseri W.: Preparation and characterization of cationic nanofibrillated cellulose from etherification and high-shear disintegration processes. *Cellulose*, **18**, 1391–1406 (2011).
<https://doi.org/10.1007/s10570-011-9591-2>
- [77] Dominic M., Joseph R., Begum P. M. S., Kanoth B. P., Chandra J., Thomas S.: Green tire technology: Effect of rice husk derived nanocellulose (RHNC) in replacing carbon black (CB) in natural rubber (NR) compounding. *Carbohydrate Polymers*, **230**, 115620 (2020).
<https://doi.org/10.1016/j.carbpol.2019.115620>
- [78] Abraham E., Elbi P. A., Deepa B., Jyotishkumar P., Pothan L. A., Narine S. S., Thomas S.: X-ray diffraction and biodegradation analysis of green composites of natural rubber/nanocellulose. *Polymer Degradation and Stability*, **97**, 2378–2387 (2012).
<https://doi.org/10.1016/j.polymdegradstab.2012.07.028>
- [79] Goetze J., Yarulina I., Gascon J., Kapteijn F., Weckhuysen B. M.: Revealing lattice expansion of small-pore zeolite catalysts during the methanol-to-olefins process using combined operando X-ray diffraction and UV–vis spectroscopy. *ACS Catalysis*, **8**, 2060–2070 (2018).
<https://doi.org/10.1021/acscatal.7b04129>
- [80] Roy K., Pongwisuthiruchte A., Debnath S. C., Potiyaraj P.: Application of cellulose as green filler for the development of sustainable rubber technology. *Current Research in Green and Sustainable Chemistry*, **4**, 100140 (2021).
<https://doi.org/10.1016/j.crgsc.2021.100140>
- [81] Fröhlich J., Niedermeier W., Luginsland H-D.: The effect of filler-filler and filler-elastomer interaction on rubber reinforcement. *Composites Part A: Applied Science and Manufacturing*, **36**, 449–460 (2005).
<https://doi.org/10.1016/j.compositesa.2004.10.004>
- [82] Mélé P., Angellier-Coussy H., Molina-Boisseau S., Dufresne A.: Reinforcing mechanisms of starch nanocrystals in a nonvulcanized natural rubber matrix. *Biomacromolecules*, **12**, 1487–1493 (2011).
<https://doi.org/10.1021/bm101443a>
- [83] Dufresne A.: Dynamic mechanical analysis of the interphase in bacterial polyester/cellulose whiskers natural composites. *Composite Interfaces*, **7**, 53–67 (2000).
<https://doi.org/10.1163/156855400300183588>
- [84] Barkane A., Kampe E., Platnieks O., Gaidukovs S.: Cellulose nanocrystals vs. cellulose nanofibers: A comparative study of reinforcing effects in UV-cured vegetable oil nanocomposites. *Nanomaterials*, **11**, 1791 (2021).
<https://doi.org/10.3390/nano11071791>
- [85] Chen Y., Xu C., Cao X.: Dynamic rheology studies of carboxylated butadiene–styrene rubber/cellulose nanocrystals nanocomposites: Vulcanization process and network structures. *Polymer Composites*, **36**, 623–629 (2015).
<https://doi.org/10.1002/pc.22979>
- [86] Honorato L., Dias M. L., Azuma C., Nunes R. C. R.: Rheological properties and curing features of natural rubber compositions filled with fluoromica ME 100. *Polímeros*, **26**, 249–253 (2016).
<https://doi.org/10.1590/0104-1428.2352>

- [87] Shi X., Sun S., Zhao A., Zhang H., Zuo M., Song Y., Zheng Q.: Influence of carbon black on the Payne effect of filled natural rubber compounds. *Composites Science and Technology*, **203**, 108586 (2021).
<https://doi.org/10.1016/j.compscitech.2020.108586>
- [88] Brüning K., Schneider K., Roth S. V., Heinrich G.: Kinetics of strain-induced crystallization in natural rubber: A diffusion-controlled rate law. *Polymer*, **72**, 52–58 (2015).
<https://doi.org/10.1016/j.polymer.2015.07.011>
- [89] Meera A. P., Said S., Grohens Y., Thomas S.: Nonlinear viscoelastic behavior of silica-filled natural rubber nanocomposites. *Journal of Physical Chemistry C*, **113**, 17997–18002 (2009).
<https://doi.org/10.1021/jp9020118>
- [90] Yoon B., Kim J. Y., Hong U., Oh M. K., Kim M., Han S. B., Nam J-D., Suhr J.: Dynamic viscoelasticity of silica-filled styrene-butadiene rubber/polybutadiene rubber (SBR/BR) elastomer composites. *Composites Part B: Engineering*, **187**, 107865 (2020).
<https://doi.org/10.1016/j.compositesb.2020.107865>
- [91] Yasin S., Hussain M., Zheng Q., Song Y.: Effects of ionic liquid on cellulosic nanofiller filled natural rubber bionanocomposites. *Journal of Colloid and Interface Science*, **591**, 409–417 (2021).
<https://doi.org/10.1016/j.jcis.2021.02.029>
- [92] Xu H., Ding L., Song Y., Wang W.: Rheology of end-linking polydimethylsiloxane networks filled with silica. *Journal of Rheology*, **64**, 1425–1438 (2020).
<https://doi.org/10.1122/8.0000050>
- [93] Torrado A. M., Constantinescu A., Johlitz M., Lion A.: Viscoelastic behavior of filled silicone elastomers and influence of aging in inert and hermetic environment. *Continuum Mechanics and Thermodynamics*, **36**, 333–350 (2022).
<https://doi.org/10.1007/s00161-022-01112-9>
- [94] Sariha A., Joseph K.: Effect of nano clay on the constrained polymer volume of chlorobutyl rubber nanocomposites appukkuttan. *Polymer Composites*, **36**, 2135–2139 (2015).
<https://doi.org/10.1002/pc.23124>
- [95] Kourki H., Mortezaei M., Famili M. H. N.: Filler networking in the highly nanofilled systems. *Journal of Thermoplastic Composite Materials*, **29**, 1047–1063 (2016).
<https://doi.org/10.1177/0892705714556830>
- [96] Hsissou R., Bekhta A., Dagdag O., El Bachiri A., Rafik M., Elharfi A.: Rheological properties of composite polymers and hybrid nanocomposites. *Heliyon*, **6**, e04187 (2020).
<https://doi.org/10.1016/j.heliyon.2020.e04187>
- [97] Ogunsona E., Hojabr S., Berry R., Mekonnen T. H.: Nanocellulose-triggered structural and property changes of acrylonitrile-butadiene rubber films. *International Journal of Biological Macromolecules*, **164**, 2038–2050 (2020).
<https://doi.org/10.1016/j.ijbiomac.2020.07.202>
- [98] Barghamadi M., Karrabi M., Ghoreishy M. H. R., Mohammadian-Gezaz S.: Effects of two types of nanoparticles on the cure, rheological, and mechanical properties of rubber nanocomposites based on the NBR/PVC blends. *Journal of Applied Polymer Science*, **136**, 47550 (2019).
<https://doi.org/10.1002/app.47550>
- [99] Mariano M., El Kissi N., Dufresne A.: Cellulose nanomaterials: Size and surface influence on the thermal and rheological behavior. *Polimeros*, **28**, 93–102 (2018).
<https://doi.org/10.1590/0104-1428.2413>
- [100] Nun-anan P., Wisunthorn S., Pichaiyut S., Vennemann N., Kummerlöwe C., Nakason C.: Influence of alkaline treatment and acetone extraction of natural rubber matrix on properties of carbon black filled natural rubber vulcanizates. *Polymer Testing*, **89**, 106623 (2019).
<https://doi.org/10.1016/j.polymertesting.2020.106623>
- [101] Sarkawi S. S., Dierkes W. K., Noordermeer J. W. M.: The influence of non-rubber constituents on performance of silica reinforced natural rubber compounds. *European Polymer Journal*, **49**, 3199–3209 (2013).
<https://doi.org/10.1016/j.eurpolymj.2013.06.022>
- [102] Spratte T., Plagge J., Wunde M., Klüppel M.: Investigation of strain-induced crystallization of carbon black and silica filled natural rubber composites based on mechanical and temperature measurements. *Polymer*, **115**, 12–20 (2017).
<https://doi.org/10.1016/j.polymer.2017.03.019>
- [103] Tunnichiffe L. B.: Thixotropic flocculation effects in carbon black-reinforced rubber: Kinetics and thermal activation. *Rubber Chemistry and Technology*, **94**, 298–323 (2021).
<https://doi.org/10.5254/rct.21.79896>
- [104] Kazemi H., Mighri F., Rodrigue D.: Application of nanocelluloses in rubbers. in ‘Cellulose nanoparticles: Synthesis and manufacturing’ (eds.: Thakur V. K., Frollini E., Scott J.) The Royal Society of Chemistry, Croydon 38–65 (2021).
<https://doi.org/10.1039/9781788019545-00038>
- [105] Demircan G., Kisa M., Ozen M., Aktas B.: Surface-modified alumina nanoparticles-filled aramid fiber-reinforced epoxy nanocomposites: Preparation and mechanical properties. *Iranian Polymer Journal*, **29**, 253–264 (2020).
<https://doi.org/10.1007/s13726-020-00790-z>